The following publication C. Tian, A. -T. Nguyen, E. Chung and H. Huang, "Diffusion-Driven Hybrid Unknown Input Observer for Vehicle Dynamics Estimation," in IEEE Transactions on Industrial Electronics, vol. 73, no. 4, pp. 6097-6110, April 2026 is available at https://doi.org/10.1109/TIE.2025.3626623.

Diffusion-Driven Hybrid Unknown Input Observer for Vehicle Dynamics Estimation

Cheng Tian, *Graduate Student Member, IEEE*, Anh-Tu Nguyen, *Senior Member, IEEE*, Edward Chung, and Hailong Huang, *Senior Member, IEEE*

***Abstract*—Vehicle sideslip angle (or lateral speed) and steering angle are essential variables for autonomous vehicle control and active safety systems. Existing estimation methods often depend on deterministic models or neural networks for mapping, which restricts their ability to capture vehicle dynamics distributions in complex driving conditions. This study introduces a diffusion-driven hybrid estimation framework to achieve real-time estimation of lateral speed and steering angle. The nonlinear vehicle dynamics model is represented as a linear parameter-varying (LPV) model. A score-based diffusion model is embedded into an LPV unknown input observer (UIO) to capture the multi-modal distribution of dynamics modeling uncertainty under different state-space model (SSM) parameters without retraining. The model uncertainty prediction sequences from the diffusion model are asynchronously generated to ensure real-time performance. Furthermore, we construct an end-to-end-based hybrid observer incorporating a fully-connected neural network as an expert model to identify model uncertainty for diffusion model training. Based on Lyapunov stability theory, the ℓ_∞ gain performance can be guaranteed to minimize the impacts of uncertainty approximation errors and improve the estimation quality. Experimental results obtained from a real-world test track demonstrate the consistent effectiveness of the proposed framework across various driving scenarios and different SSM parameters, especially in extreme driving scenarios outside the training data distribution. The implementation code is available at `https://github.com/tiancheng007/Diffusion-UIO`.**

***Index Terms*—Nonlinear observers, diffusion model, sideslip angle estimation, steering angle estimation, vehicle dynamics, vehicle state estimation.**

I. INTRODUCTION

PRECISE knowledge of vehicle dynamic states is essential for achieving driving safety and comfort objectives, especially in autonomous driving systems. This knowledge serves as critical information in system fault detection and diagnosis, planning and control, and active safety systems [1], [2].

The vehicle sideslip angle is defined as the arctangent of lateral speed divided by longitudinal speed. The vehicle sideslip angle represents a crucial indicator of vehicle handling and lateral stability [3]. The Electronic Stability Control (ESC) module provides longitudinal speed with ease, making the estimation of the sideslip angle directly linked to the estimation of lateral speed [4]. However, existing commercial sensors for directly measuring vehicle lateral speed, such as the ground optical flow-based Correvit S-Motion sensor and high-precision dual-antenna Global Navigation Satellite System (GNSS), cannot be widely adopted on mass-produced platforms due to cost reasons. While the sideslip angle mainly relies on lateral speed, the steering angle directly controls the vehicle direction and significantly influences vehicle lateral dynamics. The steering angle also serves as a fundamental input for autonomous vehicle motion planning module, trajectory tracking control module, and ESC systems. Typically, high-precision steering angle sensors based on absolute rotary encoders are considered fragile. While the steering angle can be measured using cost-effective analog sensors, these measurements are susceptible to conversion errors that may generate inaccurate signals [5]. Hence, alternative approaches for estimating steering angle and vehicle lateral speed hold significant value for autonomous driving systems.

Over the past two decades, vehicle lateral speed estimation using cost-effective onboard sensors has attracted widespread interest among researchers, including model-based, purely data-driven, and hybrid approaches [6]. Methods based on Kalman filters (KF) have been extensively applied in both industry and academia as state-of-the-art model-based estimation techniques. Estimators based on Unscented Kalman Filters (UKF) [7], [8] and Cubature Kalman Filters (CKF) [9], [10] typically achieve superior estimation accuracy when vehicle dynamics exhibit strong time-varying nonlinearity. Alternative model-based nonlinear observers have gained attention in recent years for their theoretical stability analysis [11]. These mainly include H-infinity observers [12], Takagi-Sugeno (TS) fuzzy unknown input observers [4], and switched TS observers [13]. Model-based methods typically require accurate knowledge of the physical system. However, precise modeling under complex driving conditions poses significant challenges.

This work was supported by PROCORE-France/Hong Kong Joint Research Scheme (F-PolyU501123 and 50785WD-PHC PROCORE 2024), and in part by Research Institute for Artificial Intelligence of Things (RIAIoT), The Hong Kong Polytechnic University via the project P0050293. *(Corresponding author: Hailong Huang).*

Cheng Tian is with the Department of Aeronautical and Aviation Engineering, The Hong Kong Polytechnic University, Hong Kong SAR, China (e-mail: cheng7.tian@connect.polyu.hk).

Anh-Tu Nguyen is with the LAMIH Laboratory, UMR CNRS 8201, and INSA Hauts-de-France, Université Polytechnique Hauts-de-France, 59300 Valenciennes, France (e-mail: tnguyen@uphf.fr).

Edward Chung is with the Department of Electrical and Electronic Engineering, and also with the Research Institute for Artificial Intelligence of Things (RIAIoT), The Hong Kong Polytechnic University, Hong Kong SAR, China (e-mail: edward.cs.chung@polyu.edu.hk).

Hailong Huang is with the Department of Aeronautical and Aviation Engineering, and also with the Research Institute for Artificial Intelligence of Things (RIAIoT), The Hong Kong Polytechnic University, Hong Kong SAR, China (e-mail: hailong.huang@polyu.edu.hk).

Data-driven methods primarily utilize measurements from onboard sensors as inputs to neural networks, which then perform deterministic mapping to obtain estimation results. The universal approximation capability of neural networks enables data-driven estimation methods to perform well under nonlinear operating conditions [14], [15]. To capture the temporal characteristics inherent in vehicle dynamics, various recurrent neural network (RNN) architectures have been extensively explored for data-driven lateral velocity estimation. Ghosh et al. [16] and Kong et al. [17] utilized long short-term memory (LSTM)-based models to capture temporal dependencies. In [18], gated recurrent units (GRUs) were applied in an end-to-end framework for mapping raw sensor data to lateral velocity estimates. A time-delay neural network architecture was introduced in [19], using principal component analysis for input selection and Kalman filtering for enhanced output smoothing. Recent research has also developed hybrid networks combining lightweight Inception V3 networks with deep LSTM regression to jointly estimate tire-road friction and sideslip angle with real-time capabilities on embedded hardware [20]. However, data-driven estimation methods exhibit limited explainability and cannot adequately guarantee generalization capabilities. For example, data-driven methods may experience performance degradation in out-of-distribution scenarios, including driving conditions with limited training data or previously unseen driving conditions [21].

Hybrid methods combine physical system knowledge with the powerful fitting capabilities of neural networks [22]. These approaches aim to constrain the neural network learning process with physical knowledge to further enhance estimation accuracy and generalization. In [23], a feedforward neural network was embedded into a reduced-order fuzzy observer to approximate unmodeled dynamics. Experimental results demonstrated that the proposed hybrid method exhibits significant advantages over model-based methods. Additionally, approaches based on Bayesian filters that utilize neural networks to provide pseudo-measurements for these filters have also been reported. In [6], a convolutional neural network (CNN) was combined with a UKF to estimate the sideslip angle through end-to-end training. Zhang et al. [24] designed an estimation scheme that integrates LSTM neural networks with an adaptive Kalman filter. Wang et al. [25] explored the potential of the KalmanNet architecture [26] for lateral velocity estimation. In [27], ridge regression methods were utilized to establish linear relationships between sensor information and vehicle states. Then the ridge regression was combined with an LSTM network with a dual-stage attention mechanism to capture residual dynamic characteristics. The above hybrid methods have demonstrated their advantages in estimation accuracy via field tests within the training data distribution.

However, in most existing studies, the measurement of the steering angle is assumed to be continuously available. This strong assumption may not be realistic due to the fragility of absolute rotary encoders and conversion errors in low-cost analog sensors. Inaccurate steering angle signals can severely impact vehicle handling and stability control, potentially causing lane deviations in autonomous vehicles during steering angle sensor faults. Existing steering angle estimation methods mostly focus on model-based estimation schemes. Considering time-varying longitudinal vehicle speed, joint estimation methods for steering angle and sideslip angle based on TS fuzzy models were proposed in [4], [5] with performance validated under smooth driving conditions. KF-based estimation techniques are also widely used for vehicle steering angle estimation. For agricultural autonomous vehicles, an adaptive KF with lever-arm compensation was developed based on GNSS and MEMS gyroscope to achieve accurate steering angle estimation [28]. A similar study was also reported in [29]. Zhang et al. [30] proposed a KF for estimating the front wheel steering angle using yaw rate, lateral acceleration, and steering motor current. Jeong et al. [31] introduced an EKF approach to identify functioning steering angle sensors in dual-redundancy EPS systems. To reduce cumulative errors in estimation, Lee et al. [32] developed a finite memory nonrecursive observer for estimating the front wheel angle. The above studies mainly examine model-based estimators that perform well under nominal conditions. However, they share key limitations: dependence on accurate system models, poor performance during aggressive maneuvers, and often reliance on GNSS. Evidence on robustness under model mismatch, GNSS-denied scenarios, and diverse driving maneuvers is still limited.

Despite significant contributions in vehicle lateral speed or steering angle estimation, research on the simultaneous estimation remains quite limited. Simultaneous estimation of steering angle and lateral speed can enhance robustness of the estimator due to their coupled dynamic relationship. Given the benefits of the hybrid estimation framework in estimating vehicle sideslip angle by combining physical knowledge and data learning, the hybrid framework offers a promising approach in vehicle dynamics estimation. However, the neural networks introduced in existing hybrid frameworks typically only perform deterministic mapping. These learning-based modules struggle to adequately capture the distribution differences in vehicle dynamic characteristics caused by varying model parameters across different vehicle types. This limitation may lead to severe performance degradation when model parameters exhibit significant mismatch. Moreover, the computational costs of existing hybrid methods are rarely reported, and the additional computational burden introduced by learning-based modules embedded in existing hybrid frameworks deserves further investigation.

To overcome the drawbacks of existing methods, this paper introduces a diffusion-driven hybrid framework to simultaneously estimate vehicle lateral speed and steering angle from only onboard available measurements. As depicted in Fig. 1, the estimation process using solely a model-based LPV unknown input observer (UIO) is first performed as the prior estimation. The available measurements v_x, r together with these prior model-based estimates $\hat{v}_y^M, \hat{\delta}_f^M$ are stacked into $\mathcal{G}$. A short-horizon sequence of $\mathcal{G}$ forms the condition sequence $\mathcal{S}$, which serves as the condition input to the embedded diffusion model. Then the diffusion model outputs the prediction sequence $\mathcal{D}$, i.e., a short-horizon sequence of modeling uncertainty estimation Γ. The prediction sequence is obtained

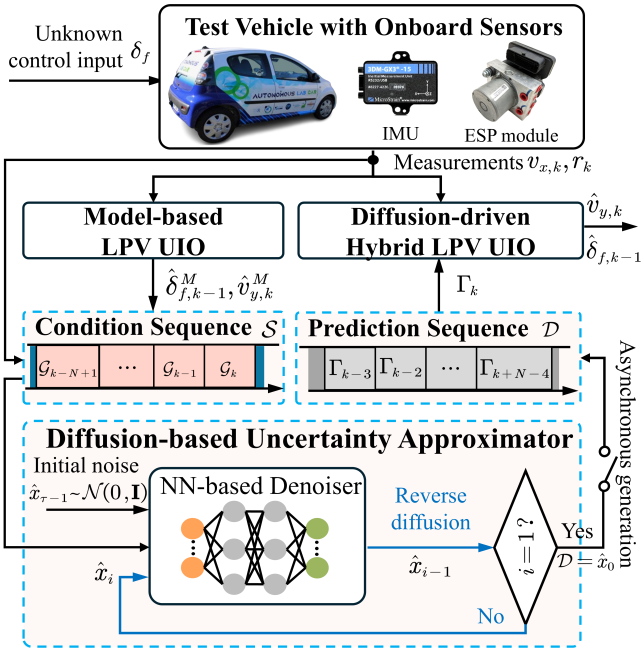

Fig. 1. Proposed diffusion-driven estimation framework.

by a reverse diffusion process: starting from Gaussian noise and iteratively denoising while being conditioned on $\mathcal{S}$. To meet real-time performance, the prediction sequence $\mathcal{D}$ is updated in an *asynchronous* loop, whereas the observer runs at the sensor rate and consumes the corresponding Γ at each time step. Specifically, the main contributions of this work are as follows.

1) A diffusion model-enhanced hybrid framework is proposed for real-time estimation of vehicle lateral speed and steering angle from the measurements of cost-effective onboard sensors. Distinguished from the existing hybrid framework using deterministic mapping [23], [27], our proposed diffusion-driven hybrid framework efficiently captures the conditional probability distribution of unmodeled vehicle dynamics across various state-space model parameters without extensive retraining.
2) We present a pioneering application of diffusion models for real-time vehicle dynamics state estimation. The implementation code of this study is accessible to facilitate the research on diffusion-based estimation approaches.
3) The diffusion model's training labels are approximated via local optimization using an end-to-end expert model with an embedded fully-connected neural network (FNN).
4) Based on Lyapunov stability theory, the disturbance caused by the approximation error of the diffusion model is minimized by means of an ℓ_∞ gain under linear matrix inequality (LMI) constraints. The performance of the proposed scheme is validated with the test data collected from a real-world test track.

Notation: I is the identity matrix with appropriate dimensions. "$\star$" denotes the symmetry term. For a matrix X, $X^\dagger$ is its Moore-Penrose pseudo-inverse, $X^\top$ is its transpose, $X \succ 0$ means that X is symmetric positive definite. We denote $\mathbb{Z}_+$ as non-negative integers and $\mathcal{I}_n = \{1, 2, \ldots, n\} \subset \mathbb{Z}_+$. For a vector x, $\|x\| = \sqrt{x^\top x}$ and $\|x\|_{\ell_\infty} = \sup_{k \geq 0} \|x_k\|$. For a scalar a, $\underline{a}$ is its lower bound, and $\bar{a}$ is its upper bound.

TABLE I
VEHICLE NOMENCLATURE

Parameter	Description
m (kg)	Vehicle mass
l_f (m)	Distance from front axle to gravity center
l_r (m)	Distance from rear axle to gravity center
I_z (kgm^2)	Moment of inertia about the z axis
C_f (N/rad)	Tire cornering stiffness (front tires)
C_r (N/rad)	Tire cornering stiffness (rear tires)
v_x (m/s)	Longitudinal speed
v_y (m/s)	Lateral speed
r (rad/s)	Yaw rate of the vehicle body
δ_f (rad)	Steering angle of the front wheel

II. VEHICLE MODELING AND PROBLEM FORMULATION

The vehicle modeling and formulated estimation problem with the unknown input are presented in this section. The vehicle nomenclature is summarized in TABLE I.

A. Vehicle Model

The single-track vehicle lateral dynamics model with the linear tire model is considered in this paper under the small angles assumption, which can be described as follows [3]:

$$\begin{aligned} \dot{v}_y &= \frac{2C_f\delta_f}{m} + \frac{2(C_r l_r - C_f l_f)r - 2(C_f + C_r)v_y}{m v_x} - r v_x \\ \dot{r} &= \frac{2C_f l_f \delta_f}{I_z} + \frac{2(C_r l_r - C_f l_f)v_y - 2(C_f l_f^2 + C_r l_r^2)r}{I_z v_x} \end{aligned} \tag{1}$$

Note that the linear tire model is effective within the linear region of lateral tire dynamics. The linear model can significantly differ from actual tire dynamics under aggressive driving with high lateral accelerations [3]. Considering modeling uncertainties, the following state-space model of the vehicle system can be obtained from (1):

$$\begin{aligned} \dot{x} &= A(v_x)x + Dd + Ww, \\ y &= Cx, \end{aligned} \tag{2}$$

where $x = [v_y, r]^\top$ is defined as the vehicle state vector, $y = r$ is the measurement vector, $d = \delta_f$ is the unknown input, w denotes the modeling uncertainties, including uncertain tire dynamics. The dimensions of the state vector, measurement vector, and unknown input vector are $n_x = 2$, $n_y = 1$, $n_d = 1$, respectively. Note that the lateral speed v_y cannot be directly measured in a mass-produced vehicle, while r and v_x are measurable. However, it is acceptable to measure the lateral speed using expensive sensors (e.g., non-contact optical sensors or high-precision GNSS) during the production stage as reference values. The state-space matrices are given by

$$\begin{aligned} A(v_x) &= \begin{bmatrix} -\frac{2(C_f + C_r)}{m v_x} & \frac{2(C_r l_r - C_f l_f)}{m v_x} \\ \frac{2(C_r l_r - C_f l_f)}{v_x I_z} & -\frac{2(C_f l_f^2 + C_r l_r^2)}{v_x I_z} \end{bmatrix}, \\ W &= I_{n_x \times n_x}, \quad C = \begin{bmatrix} 0 & 1 \end{bmatrix}, \quad D = \begin{bmatrix} \frac{2C_f}{m}, \frac{2C_f l_f}{I_z} \end{bmatrix}^\top. \end{aligned} \tag{3}$$

Based on the Euler's discretization method, the discrete-time form of the state-space model (2) with a sampling time $T_s = 0.01$ s can be expressed as

$$\begin{aligned} x_{k+1} &= A_d x_k + D_d d_k + W_d w_k, \\ y_k &= C x_k, \end{aligned} \tag{4}$$

where z_k denotes the value of any signal z taken at the instant k, $A_d = T_s A(v_x) + I$, $D_d = T_s D$ and $W_d = T_s W$.

B. Estimation Problem Statement

Two time-varying parameters (i.e., v_x and $1/v_x$) in the defined LPV vehicle system model (4) need to be considered. Based on the physical vehicle system limitations under normal driving scenarios, the measurable vehicle longitudinal speed can be bounded as follows [4]:

$$v_x \in [\underline{v}_x, \bar{v}_x], \tag{5}$$

where $\underline{v}_x = 5$ m/s, $\bar{v}_x = 30$ m/s. We represent the time-varying parameter space such that it is encompassed by a convex hull formed with three vertices [33]. Consequently, the following polytopic LPV vehicle model can be formulated from (4):

$$\begin{aligned} x_{k+1} &= \sum_{i=1}^{n_v} h_i(v_{x,k}) A_{d,i} x_k + D_d d_k + \Gamma_k + W_d \varepsilon_k, \\ y_k &= C x_k, \end{aligned} \tag{6}$$

where $n_v = 3$ is the number of vertices in defined polytopic LPV system, $\Gamma_k = [\Delta f_{1,k}, \Delta f_{2,k}]^\top$ is the estimation of modeling uncertainties by data-driven methods (e.g., FNN or proposed diffusion model), ε_k is the approximation error of the modeling uncertainty. Note that $W_d w_k = \Gamma_k + W_d \varepsilon_k$ and ε_k is assumed to be bounded in amplitude. For $i \in \mathcal{I}_3$, the local matrices $A_{d,i}$ are given by

$$\begin{aligned} A_{d,1} &= A\left(\underline{v}_x, 1/\underline{v}_x\right), \\ A_{d,2} &= A\left(\underline{v}_x, 1/\bar{v}_x\right), \\ A_{d,3} &= A\left(\bar{v}_x, 1/\bar{v}_x\right). \end{aligned} \tag{7}$$

The membership functions $h_i(v_{x,k})$ can be defined as [33]

$$\begin{bmatrix} \underline{v}_x & \underline{v}_x & \bar{v}_x \\ 1/\underline{v}_x & 1/\bar{v}_x & 1/\bar{v}_x \\ 1 & 1 & 1 \end{bmatrix} \begin{bmatrix} h_1(v_{x,k}) \\ h_2(v_{x,k}) \\ h_3(v_{x,k}) \end{bmatrix} = \begin{bmatrix} v_{x,k} \\ 1/v_{x,k} \\ 1 \end{bmatrix}. \tag{8}$$

Note that the membership functions $h_i(v_{x,k})$ satisfy the following convex sum property:

$$0 \leq h_i(v_{x,k}) \leq 1, \quad \sum_{i=1}^{n_v} h_i(v_{x,k}) = 1. \tag{9}$$

Let $\mathscr{H}$ be the set of membership functions that satisfy (9), we have

$$\begin{aligned} h &= \left[h_1(v_{x,k}), h_2(v_{x,k}), ..., h_{n_v}(v_{x,k})\right]^\top, \\ h_+ &= \left[h_1(v_{x,k+1}), h_2(v_{x,k+1}), ..., h_{n_v}(v_{x,k+1})\right]^\top, \end{aligned} \tag{10}$$

where $h, h_+ \in \mathscr{H}$. It is also important to note that the vehicle model (6) verifies the following rank conditions:

$$\operatorname{rank}(CD_d) = \operatorname{rank}(D_d), \quad \operatorname{rank} \begin{bmatrix} I_{n_x \times n_x} & D_d \\ C & 0 \end{bmatrix} = n_x + n_d. \tag{11}$$

Remark 1: Note that a standard notation is used in LPV framework in (10). h is the vector of n_v membership functions, which depend on the value of the longitudinal speed taken at instant k, and h_+ is the vector of the same n_v membership functions, which depend on the value of the longitudinal speed taken at instant $(k+1)$. Since the membership functions at instant k or instant $(k+1)$ must verify (9), it is clear that both h and h_+ belong to $\mathscr{H}$. The theoretical foundation for adopting the form of membership functions $h_i(v_{x,k})$ is based on the Barycentric coordinates. The relation (8) verifies such Barycentric coordinates.

This paper aims to develop a robust estimation algorithm for the following vehicle dynamics estimation problem.

Problem 1: Design a hybrid LPV UIO to simultaneously estimate the lateral speed v_y and the steering angle δ_f, where the modeling uncertainty distribution under different SSM parameters is approximated by the designed diffusion model.

III. DIFFUSION-DRIVEN HYBRID LPV UIO DESIGN

This section first presents the design process of an LPV UIO with a guaranteed ℓ_∞ gain performance. Then, the details on modeling uncertainty learning via the designed diffusion model are described.

A. LMI-Based LPV UIO Deisgn

To simultaneously estimate the vehicle lateral speed and steering angle, the following LPV UIO is considered:

$$\begin{aligned} \zeta_{k+1} &= \Lambda \hat{\Phi}_k + \mathcal{M}\left(h\right)^{-1} L\left(h\right)\left(y_k - C\hat{x}_k\right) \\ \hat{x}_k &= \zeta_k + \Omega y_k \\ \hat{d}_{k-1} &= (CD_d)^\dagger (y_k - C\hat{\Phi}_{k-1}) \end{aligned} \tag{12}$$

where

$$\begin{bmatrix} \mathcal{M}(h) & L(h) \end{bmatrix} = \sum_{i=1}^{n_v} h_i(v_{x,k}) \begin{bmatrix} \mathcal{M}_i & L_i \end{bmatrix}, \tag{13}$$

and $\hat{\Phi}_k = A_d(h)\hat{x}_k + \Gamma_k$, with $A_d(h) = \sum_{i=1}^{n_v} h_i(v_{x,k}) A_{d,i}$. The observer gain matrices $\mathcal{M}(h)$, $\Lambda \in \mathbb{R}^{n_x \times n_x}$, and $L(h)$, $\Omega \in \mathbb{R}^{n_x \times n_y}$ are to be designed with

$$\Lambda + \Omega C = I, \quad \Lambda D_d = 0. \tag{14}$$

Remark 2: The unknown input decoupling constraints in (14) should be satisfied to decouple the influence of unknown input on state estimation error. For the bounded ranges of model uncertainty Γ_k and model error ε_k in (6), Γ_k and ε_k are physically bounded due to the physical limations of the vehicle sytem. However, one of the major interests of the proposed method is that we do not require explicitly their bounds for theoretical developments while we can rigorously ensure the estimation performance via ℓ_∞ gain performance. This is not the case with many estimation methods [34], [35].

Consider the state estimation error $e_k = x_k - \hat{x}_k$. Then, the error dynamics can be defined from (6) and (12) as

$$e_{k+1} = \left(\Lambda A_d\left(h\right) - \mathcal{M}\left(h\right)^{-1} L\left(h\right) C\right) e_k + \Lambda W_d \varepsilon_k. \tag{15}$$

The estimation error of the unknown input can be defined as $\rho_k = \hat{d}_k - d_k$. Since $\Phi_k = A_d(h)\hat{x}_k + \Gamma_k + W_d\varepsilon_k$, then it follows that

$$\rho_k = \hat{d}_k - d_k = (CD_d)^{\dagger}C(A_d(h)e_k + W_d\varepsilon_k). \tag{16}$$

The vector of estimation errors can be formulated as follows:

$$\phi_k = \begin{bmatrix} e_k \\ \rho_k \end{bmatrix} = \begin{bmatrix} I & 0 \\ (CD_d)^{\dagger}CA_d(h) & (CD_d)^{\dagger}CW_d \end{bmatrix}\xi_k, \tag{17}$$

where $\xi_k = \begin{bmatrix} e_k^{\top} & \varepsilon_k^{\top} \end{bmatrix}^{\top}$.

The following lemmas are useful to design the proposed LPV UIO.

Lemma 1 (see [36]): Consider the membership function-dependent inequality

$$\Xi_{hhh_+} = \sum_{i=1}^{n_v}\sum_{j=1}^{n_v}\sum_{l=1}^{n_v} h_i(v_{x,k})h_j(v_{x,k})h_l(v_{x,k+1})\Xi_{ijl} \succ 0, \tag{18}$$

where Ξ_{ijl} are the symmetric matrices of appropriate dimensions that are linearly dependent on the unknown decision variables, $i, j, l \in \mathcal{I}_{n_v}$. The inequality (18) holds if

$$\begin{aligned} &\Xi_{iil} \succ 0, \quad i, l \in \mathcal{I}_{n_v}, \\ &\frac{2}{n_v - 1}\Xi_{iil} + \Xi_{ijl} + \Xi_{jil} \succ 0, \quad i, j, l \in \mathcal{I}_{n_v}, \quad i \neq j. \end{aligned} \tag{19}$$

Lemma 2 (see [37]): Let the matrices $\mathcal{A}$ and $\mathcal{B}$ given with appropriate dimensions. Then, there exists a matrix $\mathcal{X}$ satisfying $\mathcal{X}\mathcal{A} = \mathcal{B}$ if and only if $\mathcal{B}\mathcal{A}^{\dagger}\mathcal{A} = \mathcal{B}$. Moreover, the general solution of $\mathcal{X}\mathcal{A} = \mathcal{B}$ can be written as

$$\mathcal{X} = \mathcal{B}\mathcal{A}^{\dagger} + \mathcal{Y}(I - \mathcal{A}\mathcal{A}^{\dagger}), \tag{20}$$

where $\mathcal{Y}$ is an arbitrary matrix with appropriate dimensions.

The following theorem provides sufficient LMI conditions to ensure the global uniform ℓ_∞ stability of the state error system (15).

Theorem 1: If there exist matrices $P_i \in \mathbb{R}^{n_x \times n_x}$ satisfying $P_i \succ 0$, Λ, Ω satisfying the condition (14), $\mathcal{M}_i \in \mathbb{R}^{n_x \times n_x}$, $L_i \in \mathbb{R}^{n_x \times n_y}$, and positive scalars $p \leq 1$, λ, μ, then the global uniform ℓ_∞ stability of system (15) can be guaranteed with a minimal $\gamma = \sqrt{\lambda + \mu}$ by solving following LMI-based optimization problem:

$$\min(\lambda + \mu) \ \text{ subject to} \tag{21a}$$

$$\Psi_{iil} \succ 0 \tag{21b}$$

$$\frac{2}{n_v - 1}\Psi_{iil} + \Psi_{ijl} + \Psi_{jil} \succ 0 \tag{21c}$$

$$\begin{bmatrix} P_i & \star & \star & \star \\ 0_{n_x \times n_x} & \mu I_{n_x \times n_x} & \star & \star \\ I_{n_x \times n_x} & 0_{n_x \times n_x} & I_{n_x \times n_x} & \star \\ (CD_d)^{\dagger}CA_{di} & (CD_d)^{\dagger}CW_d & 0_{n_y \times n_x} & I_{n_y \times n_y} \end{bmatrix} \succeq 0 \tag{21d}$$

for $i, j, l \in \mathcal{I}_{n_v}, i \neq j$, where the quantity Ψ_{ijl} is given by

$$\Psi_{ijl} = \begin{bmatrix} (1-p)P_i & \star & \star \\ 0_{n_x \times n_x} & p\lambda I_{n_x \times n_x} & \star \\ \mathcal{M}_i\Lambda A_j - L_iC & \mathcal{M}_i\Lambda W_d & \mathcal{M}_i + \mathcal{M}_i^{\top} - P_l \end{bmatrix}.$$

Algorithm 1 LPV UIO Design with ℓ_∞ gain performance

```
Input: LPV system (6)
Output: LPV UIO (12) with the global uniform $\ell_\infty$ stability
    of error system (15)
if rank condition (11) is verified then
    Compute observer gain matrices $\Lambda$, $\Omega$ with (25)
    Solve LMI conditions (21) to get $\mathcal{M}_i$ and $L_i$
    Obtain $\mathcal{M}(h)$ and $L(h)$ from (13)
    Construct LPV UIO as (12)
else
    Not applicable for the target problem
end if
```

Proof. To compute Λ and Ω, we rewrite (14) in the following compact form:

$$\begin{bmatrix} \Lambda & \Omega \end{bmatrix}\begin{bmatrix} I & D_d \\ C & 0 \end{bmatrix} = \begin{bmatrix} I & 0 \end{bmatrix}. \tag{22}$$

Based on the rank condition (11), the solution of (22) exists. Then, we denote

$$\mathcal{A} = \begin{bmatrix} I & D_d \\ C & 0 \end{bmatrix}, \ \mathcal{B} = \begin{bmatrix} I & 0 \end{bmatrix}, \ \mathcal{X} = \begin{bmatrix} \Lambda & \Omega \end{bmatrix} \tag{23}$$

Applying Lemma 2 with (23), Λ and Ω can be calculated by

$$\begin{aligned} \begin{bmatrix} \Lambda & \Omega \end{bmatrix} = &\begin{bmatrix} I & 0 \end{bmatrix}\begin{bmatrix} I & D_d \\ C & 0 \end{bmatrix}^{\dagger} \\ &+ \mathcal{Y}\left(I - \begin{bmatrix} I & D_d \\ C & 0 \end{bmatrix}\begin{bmatrix} I & D_d \\ C & 0 \end{bmatrix}^{\dagger}\right), \end{aligned} \tag{24}$$

where $\mathcal{Y}$ is an arbitrary matrix with appropriate dimensions. Selecting $\mathcal{Y} = 0$, the explicit solutions of Λ, Ω are given by

$$\Lambda = I - D_d(CD_d)^{\dagger}C, \quad \Omega = D_d(CD_d)^{\dagger}. \tag{25}$$

Applying Lemma 1, it follows from (21b) and (21c) that

$$\begin{bmatrix} (1-p)P(h) & \star & \star \\ 0 & p\lambda I & \star \\ \mathcal{M}(h)\Lambda A(h) - L(h)C & \mathcal{M}(h)\Lambda W_d & \mathscr{M}(h, h_+) \end{bmatrix} \succ 0, \tag{26}$$

where $\mathscr{M}(h, h_+) = \mathcal{M}(h) + \mathcal{M}(h)^{\top} - P(h_+)$. Since $P(h_+) \succ 0$, it implies that $\mathcal{M}(h) + \mathcal{M}(h)^{\top} \succ 0$. Thus, we can conclude that $\mathcal{M}(h)^{-1}$ exists. Following similar arguments as in the proof of [33, Theorem 1], we can prove that conditions (26) and (21d) ensure the global uniform ℓ_∞ stability of system (15) with the following ℓ_∞-gain performance:

$$\lim_{k \to \infty} \sup||\phi_k|| \leq \gamma||\varepsilon||_{\ell_\infty}. \tag{27}$$

Note that the performance level $\gamma = \sqrt{\lambda + \mu}$ is minimized to attenuate the peak-to-peak disturbance effect of ε_k on the estimation errors. ☐

The design process of proposed LPV UIO is summarized in Algorithm 1.

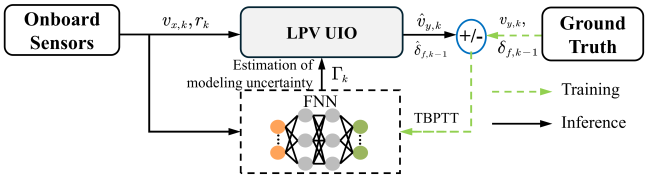

Fig. 2. End-to-end expert approximator for training label generation.

B. Diffusion-Based Modeling Uncertainty Learning

In this work, the powerful data distribution learning capability of diffusion models is leveraged in vehicle state estimation problems. The denoising process of the designed diffusion model is conditioned on the available measurements v_x, r and the prior estimates $\hat{v}_y^M, \hat{\delta}_f^M$ output by the model-based LPV UIO (Section III-A). Specifically, the diffusion model is designed to generatively learn the data distribution of modeling uncertainties in the vehicle dynamic model when there is a mismatch between the assumed SSM parameters and real-world data. The details are presented below.

1) Training Dataset Generation via End-to-End Manner: To ensure real-time estimation performance of the proposed diffusion-driven observer, we formulate the prediction of Γ as an asynchronous sequence generation problem. For a time window of length N, the condition sequence $\mathcal{S}$ and the uncertainty prediction sequence $\mathcal{D}$ are defined as follows:

$$\mathcal{S} = [\mathcal{G}_{k-N+1}, \cdots, \mathcal{G}_k], \quad \mathcal{D} = [\Gamma_k, \cdots, \Gamma_{k+N-1}], \tag{28}$$

where $\mathcal{G}_k = \left[v_{x,k}, r_k, \hat{v}_{y,k}^M, \hat{\delta}_{f,k-1}^M \right]^\top$. Note that while $\mathcal{D} = [\Gamma_k, \cdots, \Gamma_{k+N-1}]$ is generated asynchronously at time step k, the uncertainty prediction Γ_{k+p} at the current time step $(k+p)$ can be extracted from $\mathcal{D}$ in real time.

Considering (12), the lumped modeling uncertainties can simultaneously affect the estimation accuracy of both state variables and unknown inputs. Therefore, rather than employing inverse dynamics for a direct solution, we propose embedding a fully-connected neural network (FNN) into the LPV UIO designed in Section III-A. This FNN-based UIO serves as an expert model to approximate the lumped modeling uncertainties in an end-to-end manner, which can generate labeled data for subsequent diffusion model training. The Truncated Backpropagation Through Time (TBPTT) algorithm [26] is adopted to optimize this expert model. The training process utilizes the following loss function:

$$\mathcal{L}_{Exp}(\Theta) = \frac{1}{MT} \sum_{j=1}^{M} \sum_{k=1}^{T} \left\| \hat{\vartheta}_\Theta - \vartheta \right\|^2, \tag{29}$$

where M is the number of sequences of the training dataset, T is the training sequence length, $\hat{\vartheta}_\Theta = \left[\hat{v}_{y,k}^\Theta, \hat{\delta}_{f,k-1}^\Theta \right]$ denotes the lateral speed and front wheel steering angle estimated by the expert model with trainable parameters Θ, respectively, and ϑ denotes the corresponding training label. Note that the inputs for the embedded feedforward neural network are available measurements v_x, r. The framework of the expert model is summarized in Fig. 2.

TABLE II
SSM PARAMETERS OF LPV UIO FOR EXPERT MODEL TRAINING

Parameter	**Description**	**100%**	**85%**	**110%**
m (kg)	Vehicle mass	1077	915.45	1184.7
l_f (m)	Distance from front axle to gravity center	1.08	1.08	1.08
l_r (m)	Distance from rear axle to gravity center	1.24	1.24	1.24
I_z (kgm^2)	Moment of inertia about the z axis	1442	1225.7	1586.2
C_f (N/rad)	Tire cornering stiffness (front tires)	47135	47135	47135
C_r (N/rad)	Tire cornering stiffness (rear tires)	56636	56636	56636

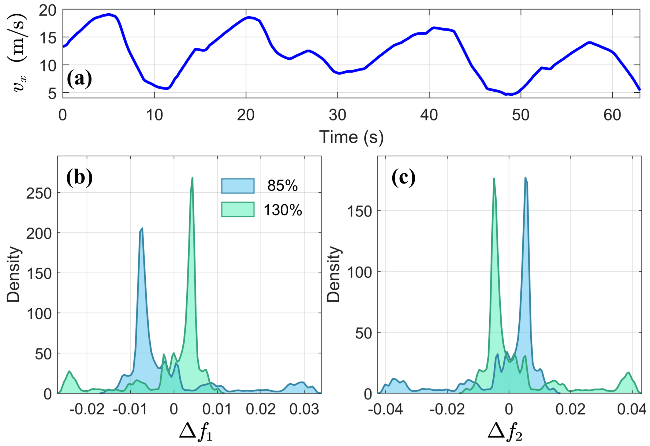

Fig. 3. End-to-end approximated modeling uncertainty distribution under *zigzag* driving maneuver. (a) Longitudinal speed, (b) Distribution of Δf_1, (c) Distribution of Δf_2.

To enable the diffusion model to capture the conditional distribution of uncertainties $p(\mathcal{D}|\mathcal{S})$ under different SSM parameters in training data, a proportional scaling strategy is applied to both m and I_z in the nominal vehicle model considering the frequent variations in vehicle load. Expert models optimized via (29) are separately trained to approximate lumped modeling uncertainties under various scale levels. Fig. 3 illustrates the lumped modeling uncertainty distributions under varying scale levels of SSM parameters approximated by the trained expert model. The longitudinal vehicle speed varies dynamically from 4.7 m/s to 19 m/s as depicted in Fig. 3(a). The modeling uncertainties exhibit distinct multi-modal characteristics under different vehicle system parameters.

Remark 3: Given the design parameter range for the Citroën C1 test vehicle's load level (curb weight 805 kg and gross weight 1190 kg, i.e., 74.7% to 110.5% of nominal vehicle mass), the SSM parameters m and I_z are scaled by 85% and 110% for the expert model training. A dedicated expert model is trained for each target scaling factor combination (i.e., 85% and 110% scale level). Note that although explicit labels for modeling uncertainty output by FNN in Fig. 2 are unavailable, the end-to-end training framework enables implicit learning of uncertainty patterns through indirect optimization. The collected real-world data is considered to contain only operating data corresponding to the nominal SSM parameters. SSM parameters of the model-based LPV UIO for the expert model training are specified in TABLE II. Further explanation is detailed in the implementation details of Section IV-A.

2) Training (Forward Diffusion Process): We denote x_0 as the training label of the uncertainty prediction sequence $\mathcal{D}$. The forward diffusion process can be described as the original data sample x_0 is gradually added with Gaussian noise in K steps according to a variance schedule β_i to form $x_0, \cdots, x_K$. Finally, x_K is approximately pure Gaussian noise. Based on the additivity of the Gaussian distribution, a noised sample can be directly calculated by the following closed-form equation:

$$x_t = \sqrt{\eta_t} x_0 + \sqrt{1-\eta_t} \epsilon_t, \tag{30}$$

where $\eta_t = \prod_{i=1}^{t}(1-\beta_i)$ is a function of decreasing noise schedule, $\epsilon_t \sim \mathcal{N}(0, \mathbf{I})$ is a random noise sample, $t \in \{1, 2, ..., K\}$, K is the number of forward diffusion steps.

Instead of training a neural network as a noise predictor, the proposed diffusion-based approximator is equivalently trained by minimizing the following MSE loss between the denoised sample and the initial sample:

$$\mathcal{L}_D(\psi) = \mathbb{E}_{\epsilon \sim \mathcal{N}(0,\mathbf{I}), t \in [1,K], x_0 \sim q(x_0)} ||x_\psi (x_t, \mathcal{S}, t) - x_0||^2, \tag{31}$$

where x_ψ denotes a neural denoiser with trainable parameters ψ, $q(x_0)$ is the given training data distribution. Note that the aim of the neural denoiser is to remove the noise in a noised sample x_t to predict the original sample $\hat{x}_0$.

3) Online Inference (Reverse Diffusion Process): The aim of the reverse diffusion process is to solve an implicit ordinary differential equation (ODE) trajectory from a random Gaussian noise sample back to the target data sample (i.e., the uncertainty prediction sequence $\mathcal{D}$) using a trained neural denoiser x_ψ under given conditional inputs. In classical diffusion model architectures, the first-order Euler method is typically employed to solve the implicit ODE in the reverse diffusion process. However, the sampling accuracy of the first-order Euler method depends on the use of small step sizes. Therefore, we adopt the second-order Heun method [38] to ensure high sample quality with a low number of inference sampling steps. Compared to the Euler method, the Heun method enhances solution accuracy by combining the prediction step and the correction step. Given total inference time steps τ, let $\hat{x}_{\tau-1} \sim \mathcal{N}(0, \mathbf{I})$ be the initial input noise. The sample update steps based on the second-order Heun method can be expressed as follows:

$$\hat{d}_i = -t_i \cdot f_s (\hat{x}_i, \mathcal{S}, t_i), \tag{32a}$$

$$\hat{x}'_{i-1} = \hat{x}_i + (t_{i-1} - t_i) \cdot \hat{d}_i, \tag{32b}$$

$$\hat{d}'_i = -t_{i-1} \cdot f_s \left(\hat{x}'_{i-1}, \mathcal{S}, t_{i-1}\right), \tag{32c}$$

$$\hat{x}_{i-1} = \hat{x}_i + \left(\hat{d}_i + \hat{d}'_i\right)(t_{i-1} - t_i)/2, \tag{32d}$$

where $f_s = (x_\psi (\hat{x}_i, \mathcal{S}, t_i) - \hat{x}_i)/t_i^2$ is the score function that provides gradient information of the target data distribution, $\hat{x}'_{i-1}$ is the priori estimate based on Euler method. To use relatively short step sizes at low noise levels, t_i is designed as the nonlinear time step schedule from [38], which can be defined as

$$t_i = \sigma(t_i) = \left(\sigma_{\min}^{1/\alpha} + \frac{i}{\tau-1}\left(\sigma_{\max}^{1/\alpha} - \sigma_{\min}^{1/\alpha}\right)\right)^{\alpha}, \tag{33}$$

where $i \in \{\tau-1, \cdots, 0\}$, $\alpha = 7$. $\sigma_{\max}, \sigma_{\min}$ are predefined maximum and minimum noise levels, respectively.

Algorithm 2 Diffusion-Driven Hybrid LPV UIO

```
Require: Denoiser $x_\psi$, observer gains $\mathcal{M}(h), L(h), \Lambda, \Omega$
Initialise: Condition sequence $\mathcal{S} = \emptyset$, prediction sequence
    $\mathcal{D} = \emptyset$, sequence index $p = 0$, Inf_Task time step $t_b = 0$
Output: $\hat{v}_{y,k}$, $\hat{\delta}_{f,k-1}$
 1: while measurements $v_{x,k}, r_k$ are not None do
 2:     Obtain sensor measurements $v_{x,k}, r_k$, current step $k$
 3:     Update condition sequence $\mathcal{S} \leftarrow v_{x,k}, r_k$
 4:     Update $\hat{v}^M_{y,k}$, $\hat{\delta}^M_{f,k-1}$ using (12) by setting $\Gamma_k = 0$
 5:     Update condition sequence $\mathcal{S} \leftarrow \hat{v}^M_{y,k}$, $\hat{\delta}^M_{f,k-1}$
 6:     if not Computing then
 7:         Inf_Task = StartReverseDiffusion($x_\psi$) using (32)
 8:         Set Computing = TRUE, $t_b = 0$
 9:     end if
10:     if Computing and IsTaskComplete(Inf_Task) then
11:         Update $\mathcal{D} \leftarrow \hat{x}_0$, $p \leftarrow t_b$
12:         Set Computing = FALSE
13:     end if
14:     Update $\Gamma_k \leftarrow \mathcal{D}[p]$
15:     Update $t_b \leftarrow t_b + 1$, $p \leftarrow p + 1$
16:     if $k > N$ then
17:         Update $\hat{v}_{y,k}$, $\hat{\delta}_{f,k-1}$ using (12)
18:     else
19:         Update $\hat{v}_{y,k} \leftarrow \hat{v}^M_{y,k}$, $\hat{\delta}_{f,k-1} \leftarrow \hat{\delta}^M_{f,k-1}$
20:     end if
21: end while
```

Cascaded integration of diffusion models into estimation systems can reduce sampling frequencies. To address this, we implement a parallel integration of the diffusion model as detailed in Algorithm 2, allowing for asynchronous generation suitable for real-time operation.

Remark 4: The implementation process of the diffusion-driven hybrid LPV UIO is summarized as follows: **Training**: Based on the end-to-end training framework in Fig. 2, we first use collected real-world vehicle data to train two expert models at 85% and 110% scale levels of SSM parameters. The trained expert models are then used for inference on the training set to generate training labels for the designed diffusion model at 85% and 110% scale levels, respectively. Subsequently, the diffusion model is trained via (31). **Online inference**: As shown in Algorithm 2, the model-based LPV UIO first outputs prior estimates based on available measurements (line 4). Then, the measurements and prior estimates are concatenated as conditional input for the designed diffusion model (line 3, 5). When the diffusion model is not in reverse diffusion process, it invokes StartReverseDiffusion asynchronously (lines 6-9). Temporal synchronization is ensured through buffer $\mathcal{D}$, which stores time-indexed diffusion outputs. When the diffusion model is in inference mode, the required uncertainty prediction at current time step can be retrieved from the buffer of prediction sequence $\mathcal{D}$ via sequence index p (line 14-

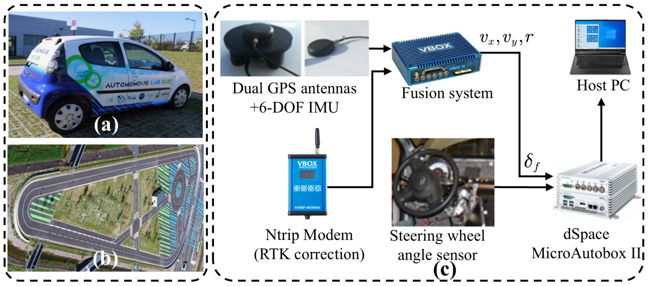

Fig. 4. Experimental facilities and test track. (a) Test vehicle, (b) Gyrovia test track in France, (c) Data acquisition system.

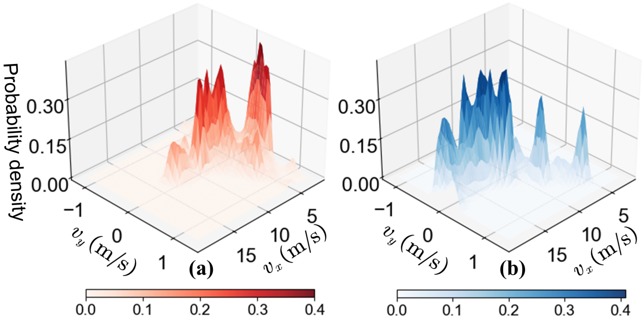

Fig. 5. Statistical analysis of dataset. (a) Training set, (b) Out-of-distribution test set.

15), which can guarantee correct temporal alignment despite asynchronous computation. This buffered asynchronous mechanism balances real-time requirements with diffusion-based enhancement.

IV. EXPERIMENTAL RESULTS

To demonstrate the effectiveness of the proposed framework, this section presents the experimental results performed on the Gyrovia test track shown in Figs. 4(a) and 4(b). The Gyrovia test track features a variety of winding routes, straight sections, a roundabout with four access points, and multiple junctions. The test track is developed on two routes with approximately 850 m, including turns with varying radii. The curvature ranges from 0 to 0.1 m^{-1}, facilitating testing from straight-line driving to sharp cornering [39]. This design allows for a comprehensive evaluation of vehicle dynamics behavior in diverse driving scenarios.

A. Experimental Setup

The experimental data were acquired using the facilities illustrated in Fig. 4(c). The test vehicle is installed with a high-precision integrated positioning system (Racelogic VBOX III), which incorporates a dual-antenna GPS enhanced with RTK correction, a 6-degree-of-freedom inertial measurement unit (IMU), and a fusion module that synthesizes measurements from both the IMU and the dual-antenna GPS. These signals are sampled at 100 Hz by the dSpace MicroAutobox II and transmitted via a CAN bus with the captured variables including δ_f, v_x, v_y, and r. To rigorously assess the performance of the proposed framework under varying conditions, the INSA autonomous vehicle executed a series of maneuvers on the test track.

1) Implementation Details: In this study, we simulated different degrees of mismatch with the actual vehicle system by scaling the nominal vehicle parameters m and I_z.

Dataset: The test vehicle conducted random smooth driving, sharp turns, and an extreme *zigzag* driving scenario that involved rapid lane changes and acceleration. The collected test vehicle data was divided into a training set, an in-distribution test set (random smooth driving, sharp turns), and an out-of-distribution test set (extreme *zigzag* driving) with ratios of **68%**, **22%**, and **10%**, respectively. The expert model for generating labels incorporates an FNN, which consists of three hidden layers with 64, 512, and 64 neurons, respectively. The input to this FNN is the available measurements at each time step. The training set was first used for expert model training, which includes random smooth driving and sharp turn driving conditions. The in-distribution test set was used for model validation during expert model training. Subsequently, expert models were trained separately under embedded LPV UIO at 85% and 110% scale levels of nominal SSM parameters. The trained expert models were then used to generate training labels for the diffusion model. For testing, we set scale levels of SSM parameters m and I_z at 75%, 100%, and 130% based on the load range of the test vehicle. As presented in Fig. 5, the out-of-distribution test set differs significantly from the distribution of the training set. The out-of-distribution test set features higher longitudinal vehicle speeds, and the vehicle dynamics exhibit strong nonlinear coupling characteristics.

Diffusion model: To demonstrate the superior performance of our proposed framework, the neural denoiser x_ψ is also simply parameterized by a standard FNN with three hidden layers of 256 neurons and Mish activation functions in each layer. The diffusion step is encoded by a neural network with two hidden layers of 128 neurons and Mish activation functions in each layer. The encoded diffusion step, noised sample, and condition sequence are then concatenated and input into the neural denoiser. The neural denoiser x_ψ is trained using the Adam optimizer with an initial learning rate of 2×10^{-4} and a mini-batch size of 256. The number of forward diffusion steps is set to $K = 1000$. We set the number of reverse diffusion steps to $\tau = 10$ for efficient online inference. The time window length for both the condition sequence and the prediction sequence is set to $N = 15$. The YALMIP package [40] with SDPT3 solver is utilized to solve the observer gains. The observer gains with $\gamma_{\min} = 0.2275$ under nominal parameters (100% scale level) are given by

$$L_1 = [-1.6809, -0.0007]^\top,\ L_2 = [-1.3221, -0.0004]^\top,$$

$$L_3 = [-1.5748, -0.0013]^\top,\ \mathcal{M}_1 = \begin{bmatrix} 1.8200 & 0.1172 \\ 0.0007 & 288.6321 \end{bmatrix},$$

$$\mathcal{M}_2 = \begin{bmatrix} 1.0105 & 0.1191 \\ -0.0004 & 288.6321 \end{bmatrix},\ \Lambda = \begin{bmatrix} 1 & -1.2397 \\ 0 & 0 \end{bmatrix},$$

$$\mathcal{M}_3 = \begin{bmatrix} 1.0105 & 0.1191 \\ -0.0004 & 288.6321 \end{bmatrix},\ \Omega = \begin{bmatrix} 1.2397 \\ 1 \end{bmatrix}.$$

2) Baseline Methods: To ensure a comprehensive evaluation, we benchmarked the following estimators:

- TS-UIO [4]: The TS fuzzy UIO is selected as the baseline model-based method. The observer gains of TS-UIO under different scale levels are specified in our code repository. Note that [4] and [33] belong to the class of model-based estimation approaches (not hybrid one), which heavily depend on the reliability of the vehicle model. Moreover, theoretically speaking, the basic model-based component LPV UIO in this paper is a simplified version (no unmeasured nonlinearities in [33]; and used for different estimation contexts) of [4]. However, both approaches utilize the same decoupling-based technique for UIO design, leading to similar drawbacks.
- E2E-UIO (adapted from [23]): The designed LPV UIO with an end-to-end approximator is selected as the baseline hybrid method. Note that it also belongs to the class of hybrid approaches combining model-based estimator and NNs using deterministic mapping. The embedded FNN in this expert model consists of three hidden layers with 32, 64, and 16 neurons, respectively. E2E-UIO is trained by Adam optimizer with an initial learning rate of 1×10^{-3} and a sequence length of 100. The embedded LPV UIO shares the same observer gains as the proposed diffusion-driven hybrid UIO.
- Diff-UIO: Proposed diffusion-driven hybrid LPV UIO.

3) Evaluation Metrics: For a comprehensive evaluation of estimation accuracy and extreme error distribution, the following evaluation metrics are selected.

RMSE: Root mean square error (RMSE) quantifies the average magnitude of prediction errors by computing the square root of the mean squared differences between predicted and actual values. RMSE is expressed as

$$\mathrm{RMSE} = \sqrt{\frac{1}{n}\sum_{k=1}^{n}(\hat{z}_k - z_k)^2}, \tag{34}$$

where, n is the number of data samples, $\hat{z}_k$ is the estimate value at step k, and z_k is the reference value at step k.

MAE: Mean absolute error (MAE) measures the average absolute deviation between predicted and ground truth values. Unlike RMSE, MAE treats all errors equally without amplifying larger deviations. MAE is expressed as

$$\mathrm{MAE} = \frac{1}{n}\sum_{k=1}^{n}|\hat{z}_k - z_k|. \tag{35}$$

AE95: 95th percentile of absolute errors represents the threshold below which 95% of all absolute errors fall. The AE95 metric is selected to complement RMSE and MAE by providing insight into the model's performance in worst-case scenarios. While RMSE and MAE are excellent measures of central tendency and average error magnitude, they can be affected by error distribution and may overlook large outliers. AE95 provides the upper limit of errors for 95% of predictions, which is essential for evaluating the reliability of the model, especially in scenarios where significant errors can have serious impacts. AE95 is expressed as

$$\mathrm{AE95} = P_{95}(\{|\hat{z}_k - z_k|\}_{k=1}^{n}), \tag{36}$$

where, P_{95} is the operation of calculating the 95th percentile.

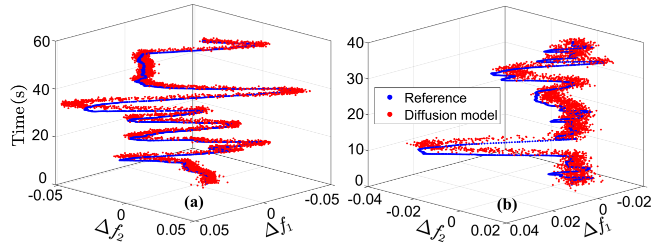

Fig. 6. Estimation of modeling uncertainty $\Gamma_k = [\Delta f_{1,k}, \Delta f_{2,k}]^\top$ (130% scale level). (a) Test 1, (b) Test 3.

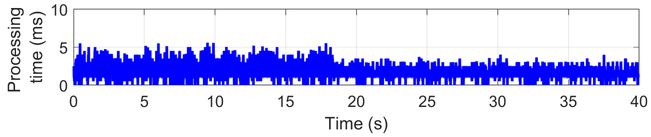

Fig. 7. Processing time of Diff-UIO under Test 3.

Remark 5: To demonstrate the estimation performance out of the training data distribution, we excluded data from the Test 3 *zigzag* extreme driving scenario when training the E2E-UIO and Diff-UIO models. Additionally, due to page limitations, only the estimation results at the 130% scale level are presented graphically. The ranges of estimated modeling uncertainty Γ_k in Test 1 and Test 3 are illustrated in Fig. 6. The reference value is approximated by the expert model. We can observe that the range of the estimated modeling uncertainty is bounded even in the out-of-distribution scenario (Test 3). In addition to directly comparing the curves of the estimation results, we also selected lateral acceleration a_y as the abscissa to graphically analyze $\delta_{f\mathrm{MAE}}, v_{y\mathrm{MAE}}$ since tire nonlinear characteristics significantly intensify as lateral acceleration a_y increases. The variation patterns can demonstrate the estimation performance under highly dynamic nonlinear driving conditions. Such analysis is important for safety-critical vehicle active safety and autonomous driving systems. The quantitative estimation results for the 75%, 100%, and 130% scale levels are summarized in TABLE IV.

Remark 6: The implementation of all the above baseline methods is based on the PyTorch deep learning framework. Using this framework, we evaluated the computational efficiency of these baseline methods on a PC (Intel i5-13490 CPU, 32-GB memory, NVIDIA RTX 4070 GPU). The results indicate that the average processing time for TS-UIO is **2.14 ms**, for E2E-UIO is **2.01 ms**, and for Diff-UIO is **1.68 ms**, while the average inference time for the designed diffusion model alone is approximately **21 ms**. Note that the model-based TS-UIO is generally recognized for its significant advantage in terms of computational complexity [6]. Python threading and NVIDIA CUDA Streams are utilized to enable asynchronous processing in our implementation of Algorithm 2. This implementation effectively emphasizes the benefits of Diff-UIO regarding real-time inference capability compared to the cascade structure. As shown in Fig. 7, the worst-case latency of the proposed Diff-UIO is about 5.60 ms, which is significantly faster than the typical 10 ms control cycle [41] used in real vehicle control systems. The two NVIDIA DRIVE AGX Orin units (508

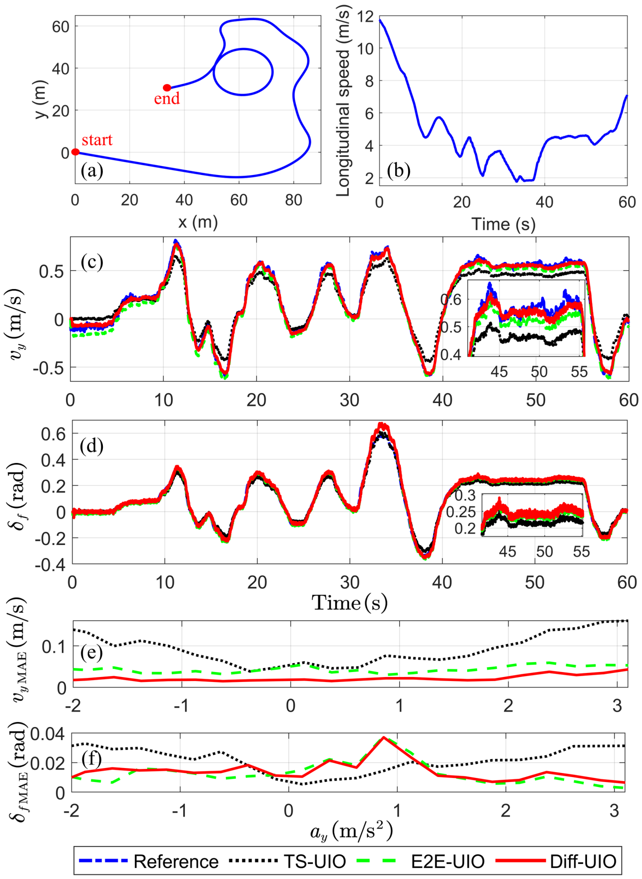

Fig. 8. Estimation results of Test 1: (a) Vehicle path, (b) Longitudinal velocity v_x, (c) Lateral velocity v_y, (d) Steering angle of the front wheel δ_f, (e) MAE of v_y, (f) MAE of δ_f. (Binsize=$0.25\mathrm{m/s}^2$, 130% SSM parameters m, I_z scaling).

TOPS) widely used in existing intelligent vehicles can provide AI computing power comparable to our computing platform (466 TOPS) used in this study, thereby meeting the real-time computing requirements of embedded systems. For practical deployment, computational efficiency can be further enhanced through model quantization techniques.

B. Test 1: Smooth Driving Scenario

Fig. 8 presents the estimation results for Test 1, which features a smooth driving scenario as illustrated by the vehicle path in Fig. 8(a). The trajectory includes multiple turns and a loop-like pattern with varying longitudinal velocity shown in Fig. 8(b). As demonstrated in Figs. 8(c) and 8(d), all estimation methods have comparable estimation performance in this scenario. The zoom-in subplots in Figs. 8(c) and 8(d) provide a detailed view of the estimation performance during a critical period. In Fig. 8(c), the zoom-in subplot reveals that the Diff-UIO method demonstrates superior tracking accuracy for lateral velocity estimation compared to the E2E-UIO approach. The performance advantage of the Diff-UIO becomes more evident in Figs. 8(e) and 8(f). The proposed Diff-UIO consistently maintains lower estimation errors compared to the baseline methods across different lateral acceleration values. Moreover, the $v_{y\mathrm{AE95}}$ in TABLE IV further supports this observation by indicating an upper error bound that is significantly lower than that of the baseline methods. The results suggest that the proposed Diff-UIO offers satisfactory estimation accuracy in normal driving conditions.

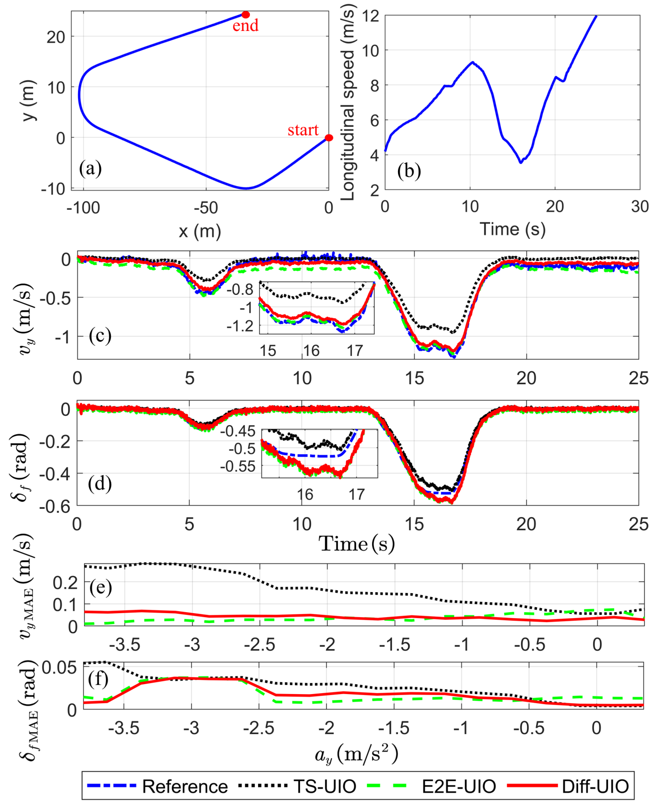

Fig. 9. Estimation results of Test 2: (a) Vehicle path, (b) Longitudinal velocity v_x, (c) Lateral velocity v_y, (d) Steering angle of the front wheel δ_f, (e) MAE of v_y, (f) MAE of δ_f. (Binsize=$0.25\mathrm{m/s}^2$, 130% SSM parameter m, I_z scaling).

C. Test 2: Sharp Turns Scenario

For this scenario, the test vehicle executed a driving sequence consisting of two abrupt cornering maneuvers followed by a period of smooth driving operation. As shown in Fig. 9(c), a distinct negative peak appears at approximately 15 s at the sharpest part of the turn. In both cases, compared to the baseline approach, the proposed Diff-UIO demonstrates superior estimation performance over TS-UIO, particularly during the most challenging moments of the sharp turn. This performance advantage is further corroborated in Figs. 9(e) and 9(f). Across the entire range of lateral acceleration, Diff-UIO consistently maintains lower estimation errors than TS-UIO. Although Diff-UIO and E2E-UIO show similar estimated trajectories in Figs. 9(c) and 9(d), the lower $v_{y\mathrm{MAE}}$ and $\delta_{f\mathrm{MAE}}$ in TABLE IV indicate that the proposed Diff-UIO achieves higher accuracy. This indicates that the diffusion-driven approach offers enhanced robustness during demanding maneuvers such as sharp turns.

D. Test 3: Extreme Driving Scenario (Out-of-Distribution)

This scenario features demanding lateral maneuvers characterized by alternating steering inputs. As data from these pro-

TABLE III
ABLATION STUDY ON DIFFUSION COMPONENT

Setting	LPV UIO	GMM	Diffusion	Test 1: Smooth Driving				Test 2: Sharp Turns				Test 3: Extreme Driving			
				$v_{y\text{RMSE}}$	$\delta_{f\text{RMSE}}$	$v_{y\text{AE95}}$	$\delta_{f\text{AE95}}$	$v_{y\text{RMSE}}$	$\delta_{f\text{RMSE}}$	$v_{y\text{AE95}}$	$\delta_{f\text{AE95}}$	$v_{y\text{RMSE}}$	$\delta_{f\text{RMSE}}$	$v_{y\text{AE95}}$	$\delta_{f\text{AE95}}$
1	✓			0.0878	0.0219	0.1419	0.0389	0.1232	0.0193	0.2789	0.0503	0.1001	0.0252	0.1970	0.0509
2	✓	✓		0.0668	0.0169	0.1225	**0.0343**	0.1002	0.0155	0.2344	0.0420	0.0890	0.0222	0.1909	0.0442
3	✓		✓	**0.0404**	**0.0169**	**0.0711**	0.0345	**0.0652**	**0.0127**	**0.1327**	**0.0316**	**0.0776**	**0.0213**	**0.1589**	**0.0418**

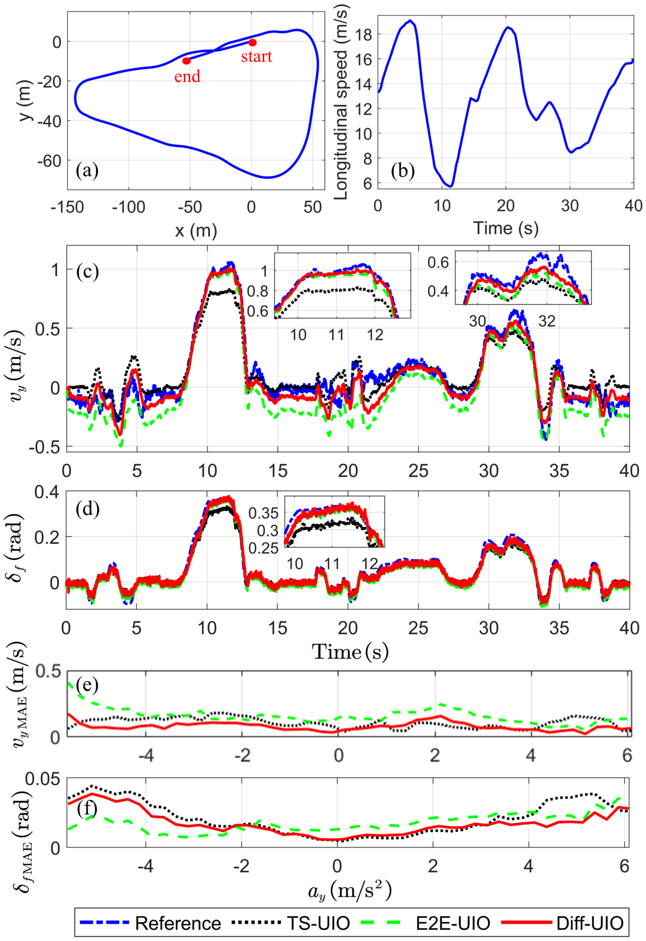

Fig. 10. Estimation results of Test 3 (**out-of-distribution**): (a) Vehicle path, (b) Longitudinal velocity v_x, (c) Lateral velocity v_y, (d) Steering angle of the front wheel δ_f, (e) MAE of v_y, (f) MAE of δ_f. (Binsize=0.25m/s^2, 130% SSM parameter m, I_z scaling).

nounced driving conditions were deliberately omitted from the training dataset, the scenario serves as an *out-of-distribution* test case.

As shown in Figs. 10(c) and 10(d), the vehicle performed multiple significant lateral dynamic changes, particularly around the 10 s and 30 s where substantial variations in lateral velocity and steering angle occur. Notably, in these high-dynamic regions, the proposed Diff-UIO demonstrates estimation results that more closely align with the reference values. In contrast, TS-UIO exhibits clear underestimation in certain peak regions, while E2E-UIO shows considerable deviations in some intervals shown in the subplot of Fig. 10(c) due to the limited generalization capability. Both $v_{y\text{RMSE}}$ and $v_{y\text{AE95}}$ for E2E-UIO in TABLE IV confirm the previous observation. These values are even substantially larger than those of TS-UIO. Figs. 10(e) and 10(f) further evaluate the performance of each method from the perspective of lateral acceleration. The probabilistic characteristics of the diffusion model enable Diff-UIO to adapt to variations in vehicle dynamics under different SSM parameter scaling levels. The lower AE95 metrics for Diff-UIO in TABLE IV further indicate that Diff-UIO maintains good estimation performance even under worst-case conditions. Given that this test scenario exceeds the training data distribution with 130% SSM parameter scaling, these results highlight the proposed Diff-UIO's superior generalization capability.

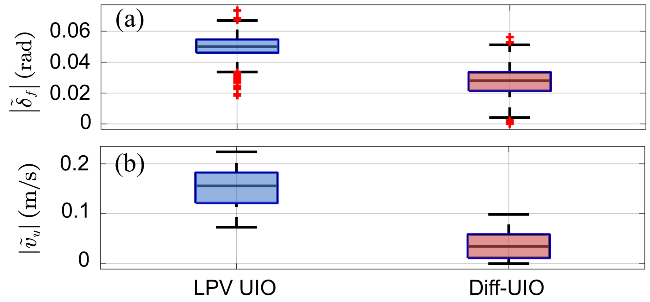

Fig. 11. Box plot of the absolute estimation error in Test 3 ($|\delta_f| \geq 0.3$ rad). (a) Error of steering angle $|\tilde{\delta}_f|$, (b) Error of lateral speed $|\tilde{v}_y|$.

E. Ablation Study

An ablation study is conducted to evaluate the contribution of the proposed diffusion component. We select Gaussian mixture model (GMM) [42] as a baseline for the probabilistic component to model the uncertainty distribution across different scales of SSM parameters. GMM is a classical probabilistic model that assumes data consists of a mixture of multiple Gaussian distributions. The number of model components is determined as 6 based on the Bayesian information criterion. The GMM-based modeling shares the same training set and conditional inputs with the diffusion component.

The test results at the 75% scale level are presented in TABLE III. Specifically, compared to the baseline LPV UIO (Setting 1), the proposed Diff-UIO (Setting 3) reduces $v_{y\text{RMSE}}$ by 54% in Test 1 and achieves a significant 47% improvement in Test 3. When compared to the GMM-based UIO (Setting 2), Setting 3 also demonstrates superior performance, with $v_{y\text{RMSE}}$ improvements of 40% and 35% in Test 1 and Test 3, respectively. Similar improvement trends can be also observed for $\delta_{f\text{RMSE}}$. By examining $v_{y\text{AE95}}$ and $\delta_{f\text{AE95}}$, Setting 3

TABLE IV
QUANTITATIVE ESTIMATION RESULTS OF TEST SCENARIOS

Scale	Metrics	Test 1: Smooth Driving			Test 2: Sharp Turns			Test 3: Extreme Driving (OOD)		
		Diff-UIO	**E2E-UIO**	**TS-UIO**	**Diff-UIO**	**E2E-UIO**	**TS-UIO**	**Diff-UIO**	**E2E-UIO**	**TS-UIO**
100%	$v_{y\mathrm{RMSE}}(\mathrm{m/s})$	**0.0311**	0.0428	0.0822	**0.0538**	0.0574	0.1191	**0.0669**	0.1187	0.0977
	$\delta_{f\mathrm{RMSE}}(\mathrm{rad})$	0.0175	**0.0170**	0.0221	**0.0134**	0.0135	0.0196	**0.0188**	0.0212	0.0243
	$v_{y\mathrm{MAE}}(\mathrm{m/s})$	**0.0257**	0.0372	0.0716	**0.0447**	0.0457	0.0901	**0.0499**	0.0934	0.0782
	$\delta_{f\mathrm{MAE}}(\mathrm{rad})$	**0.0117**	0.0125	0.0186	**0.0087**	0.0114	0.0115	**0.0146**	0.0181	0.0184
	$v_{y\mathrm{AE95}}(\mathrm{m/s})$	**0.0580**	0.0732	0.1336	**0.1016**	0.1078	0.2608	**0.1403**	0.2390	0.1955
	$\delta_{f\mathrm{AE95}}(\mathrm{rad})$	0.0380	**0.0345**	0.0390	0.0307	**0.0275**	0.0511	**0.0378**	0.0380	0.0496
75%	$v_{y\mathrm{RMSE}}(\mathrm{m/s})$	**0.0404**	0.0528	0.0776	0.0652	**0.0611**	0.1139	**0.0776**	0.1044	0.0987
	$\delta_{f\mathrm{RMSE}}(\mathrm{rad})$	0.0169	**0.0159**	0.0228	0.0127	**0.0112**	0.0201	0.0213	**0.0202**	0.0243
	$v_{y\mathrm{MAE}}(\mathrm{m/s})$	**0.0341**	0.0443	0.0676	0.0520	**0.0478**	0.0867	**0.0579**	0.0774	0.0795
	$\delta_{f\mathrm{MAE}}(\mathrm{rad})$	0.0125	**0.0113**	0.0192	**0.0077**	0.0080	0.0114	0.0166	**0.0163**	0.0184
	$v_{y\mathrm{AE95}}(\mathrm{m/s})$	**0.0711**	0.0919	0.1278	0.1327	**0.1279**	0.2484	**0.1589**	0.2130	0.1931
	$\delta_{f\mathrm{AE95}}(\mathrm{rad})$	0.0345	**0.0326**	0.0401	0.0316	**0.0262**	0.0528	**0.0418**	0.0379	0.0496
130%	$v_{y\mathrm{RMSE}}(\mathrm{m/s})$	**0.0239**	0.0486	0.0884	**0.0441**	0.0727	0.1256	**0.0860**	0.1615	0.1175
	$\delta_{f\mathrm{RMSE}}(\mathrm{rad})$	0.0200	**0.0194**	0.0215	**0.0149**	0.0186	0.0190	**0.0171**	0.0203	0.0228
	$v_{y\mathrm{MAE}}(\mathrm{m/s})$	**0.0188**	0.0427	0.0773	**0.0378**	0.0595	0.0943	**0.0649**	0.1376	0.0921
	$\delta_{f\mathrm{MAE}}(\mathrm{rad})$	0.0133	**0.0131**	0.0180	**0.0096**	0.0153	0.0117	**0.0134**	0.0178	0.0172
	$v_{y\mathrm{AE95}}(\mathrm{m/s})$	**0.0470**	0.0836	0.1422	**0.0776**	0.1379	0.2764	**0.1853**	0.3115	0.2386
	$\delta_{f\mathrm{AE95}}(\mathrm{rad})$	**0.0432**	0.0423	0.0379	**0.0379**	0.0406	0.0491	**0.0342**	0.0348	0.0474

OOD: Out-of-Distribution.

shows superior performance in capturing worst-case error scenarios across all test conditions. As shown in Fig. 11, model-based LPV UIO and Diff-UIO at scale level 75% are compared in box plots for Test 3 conditioned on large steering angles ($|\delta_f| \geq 0.3$ rad). Diff-UIO shows clearly lower medians and much tighter interquartile ranges for both estimation errors of steering angle and lateral speed, together with shorter upper whiskers and fewer outliers. This indicates that not only are the typical errors smaller, but the tail errors are also significantly reduced when the small-angle assumption is not valid. These results suggest that the proposed diffusion component is more effective at capturing unmodeled vehicle dynamics.

F. Quantitative Results Analysis

TABLE IV presents the quantitative estimation results across three driving scenarios under different scale conditions. The diffusion model-based Diff-UIO consistently demonstrates superior accuracy in most test cases.

At nominal scale (100%), Diff-UIO achieves lower $v_{y\mathrm{RMSE}}$ than both baselines in Test 1 (smooth driving). In Test 2 (sharp turns), despite reduced accuracy across all methods, Diff-UIO maintains its advantage with $\delta_{f\mathrm{RMSE}}$ approximately 28% lower than TS-UIO. Test 3 (extreme driving) highlights Diff-UIO's robustness in out-of-distribution conditions, where it substantially outperforms both baseline methods. At 75% scale, while E2E-UIO slightly outperforms Diff-UIO in Test 2, this can be attributed to the neural network's learned representations coincidentally aligning better with sharp-turn dynamics under parameter downscaling. However, Diff-UIO maintains a lower $v_{y\mathrm{AE95}}$ in Test 3, indicating more consistent overall performance. The 130% scale results further emphasize Diff-UIO's advantages, particularly in Test 3, where it achieves $v_{y\mathrm{RMSE}}$ approximately 47% lower than E2E-UIO and 27% lower than TS-UIO. This superior performance under parameter mismatch conditions demonstrates the effectiveness of the diffusion model in capturing complex system dynamics.

In summary, Diff-UIO exhibits excellent generalization across diverse scenarios and scale variations, particularly excelling in out-of-distribution conditions. While E2E-UIO shows competitive performance in specific cases and TS-UIO requires no training data, neither matches Diff-UIO's robust performance in complex driving scenarios with SSM parameter uncertainties.

V. CONCLUSION AND FUTURE WORK

This paper presents a novel diffusion-driven hybrid estimation framework for real-time estimation of vehicle lateral speed and steering angle. A diffusion model is incorporated into an LPV UIO to effectively capture the dynamics modeling uncertainty distribution under different SSM parameters without retraining. To achieve real-time performance, we design an asynchronous sampling strategy for the uncertainty prediction sequences from the diffusion model. Additionally, we successfully identify and generate high-quality model uncertainty data for diffusion model training through expert models based on an end-to-end paradigm. Then the influence of model uncertainty compensation errors is minimized via optimized ℓ_∞ gain performance. The performance of the proposed method has been validated through experiments with INSA autonomous vehicles on a real-world test track. Experimental results indicate that the proposed framework exhibits consistently satisfactory performance across various driving scenarios and different SSM parameters compared to existing model-based and hybrid methods. Notably, in extreme driving scenarios outside the training data distribution, the proposed method maintains superior generalization performance. Future work will focus on exploring applications in vehicle fault-tolerant control under extreme driving conditions.

REFERENCES

[1] Q. Shi and H. Zhang, "Fault Diagnosis of an Autonomous Vehicle With an Improved SVM Algorithm Subject to Unbalanced Datasets," *IEEE Trans. Ind. Electron.*, vol. 68, no. 7, pp. 6248–6256, Jul. 2021.

[2] Z. Li, J. Hu, B. Leng, L. Xiong, and Z. Fu, "An Integrated of Decision Making and Motion Planning Framework for Enhanced Oscillation-Free Capability," *IEEE Trans. Intell. Transp. Syst.*, vol. 25, no. 6, pp. 5718–5732, Jun. 2024.

[3] C. Tian, C. Huang, Y. Wang, E. Chung, A.-T. Nguyen, P. K. Wong, W. Ni, A. Jamalipour, K. Li, and H. Huang, "Recent Estimation Techniques of Vehicle-Road-Pedestrian States for Traffic Safety: Comprehensive Review and Future Perspectives," *IEEE Trans. Intell. Transp. Syst.*, vol. 26, no. 3, pp. 2897–2920, 2025.

[4] A.-T. Nguyen, T. Dinh, T.-M. Guerra, and J. Pan, "Takagi–Sugeno Fuzzy Unknown Input Observers to Estimate Nonlinear Dynamics of Autonomous Ground Vehicles: Theory and Real-Time Verification," *IEEE/ASME Trans. Mechatron.*, vol. 26, no. 3, pp. 1328–1338, 2021.

[5] B. Zhang, H. Du, J. Lam, N. Zhang, and W. Li, "A Novel Observer Design for Simultaneous Estimation of Vehicle Steering Angle and Sideslip Angle," *IEEE Trans. Ind. Electron.*, vol. 63, no. 7, pp. 4357–4366, Jul. 2016.

[6] A. Bertipaglia, M. Alirezaei, R. Happee, and B. Shyrokau, "An Unscented Kalman Filter-Informed Neural Network for Vehicle Sideslip Angle Estimation," *IEEE Trans. Veh. Technol.*, vol. 73, no. 9, pp. 12 731–12 746, Sep. 2024.

[7] X. Ping, S. Cheng, W. Yue, Y. Du, X. Wang, and L. Li, "Adaptive Estimations of Tyre–Road Friction Coefficient and Body's Sideslip Angle Based on Strong Tracking and Interactive Multiple Model Theories," *Proc. Inst. Mech. Eng., Part D: J. Automob. Eng.*, vol. 234, no. 14, pp. 3224–3238, Dec. 2020.

[8] Y. Zhang, M. Li, Y. Zhang, Z. Hu, Q. Sun, and B. Lu, "An Enhanced Adaptive Unscented Kalman Filter for Vehicle State Estimation," *IEEE Trans. Instrum. Meas.*, vol. 71, pp. 1–12, 2022.

[9] Y. Liu, R. Zhang, P. Shi, L. Zhao, Y. Feng, and Y. Du, "Distributed Electric Vehicle State Parameter Estimation Based on the ASO-SRGHCKF Algorithm," *IEEE Sens. J.*, vol. 22, no. 19, pp. 18 780–18 792, Oct. 2022.

[10] Y. Liu, C. Huang, D. Zhou, X. Wang, and L. Li, "Vehicle Sideslip Angle Estimation Based on Strong Tracking SCKF Considering Road Inclinations," *IEEE Trans. Veh. Technol.*, vol. 72, no. 12, pp. 15 535–15 547, Dec. 2023.

[11] A.-T. Nguyen, L. Frezzatto, T.-M. Guerra, and S. Delprat, "Cost-Effective Estimation of Vehicle Lateral Tire-Road Forces and Sideslip Angle via Nonlinear Sampled-Data Observers: Theory and Experiments," *IEEE/ASME Trans. Mechatron.*, vol. 29, no. 6, pp. 4606–4617, 2024.

[12] B. Boada, F. Viadero-Monasterio, H. Zhang, and M.-J. Boada, "Simultaneous Estimation of Vehicle Sideslip and Roll Angles Using an Integral-Based Event-Triggered $\mathscr{H}_\infty$ Observer Considering Intravehicle Communications," *IEEE Trans. Veh. Technol.*, vol. 72, no. 4, pp. 4411–4425, Apr. 2023.

[13] Q. Zhang, H. Jing, Z. Liu, Y. Jiang, and M. Gu, "A Novel PWA Lateral Dynamics Modeling Method and Switched T-S Observer Design for Vehicle Sideslip Angle Estimation," *IEEE Trans. Ind. Electron.*, vol. 69, no. 2, pp. 1847–1857, Feb. 2022.

[14] S. Melzi and E. Sabbioni, "On the Vehicle Sideslip Angle Estimation through Neural Networks: Numerical and Experimental Results," *Mech. Syst. Signal Process.*, vol. 25, no. 6, pp. 2005–2019, Aug. 2011.

[15] A. Bonfitto, S. Feraco, A. Tonoli, and N. Amati, "Combined Regression and Classification Artificial Neural Networks for Sideslip Angle Estimation and Road Condition Identification," *Veh. Syst. Dyn.*, vol. 58, no. 11, pp. 1766–1787, Nov. 2020.

[16] J. Ghosh, A. Tonoli, and N. Amati, "A Deep Learning based Virtual Sensor for Vehicle Sideslip Angle Estimation: Experimental Results," in *Proc. SAE Int. WCX Congr. Experience*, pp. 456–463, Warrendale, PA, Apr. 2018.

[17] D. Kong, W. Wen, R. Zhao, Z. Lv, K. Liu, Y. Liu, and Z. Gao, "Vehicle Lateral Velocity Estimation Based on Long Short-Term Memory Network," *World Electr. Veh. J.*, vol. 13, no. 1, pp. 1–14, Jan. 2022.

[18] S. Srinivasan, I. Sa, A. Zyner, V. Reijgwart, M. Valls, and R. Siegwart, "End-to-End Velocity Estimation for Autonomous Racing," *IEEE Rob. Autom. Lett.*, vol. 5, no. 4, pp. 6869–6875, Oct. 2020.

[19] J. Liu, Z. Wang, and L. Zhang, "A Time-delay Neural Network of Sideslip Angle Estimation for In-wheel Motor Drive Electric Vehicles," in *Proc. IEEE 91st Veh. Technol. Conf.*, pp. 1–5, May. 2020.

[20] D. Meng, H. Chu, M. Tian, W. Shi, B. Gao, and H. Chen, "Hybrid Networks for Real-Time Vehicle Dynamic State Estimation: Simulation and Experimentation," *IEEE Trans. Ind. Electron.*, pp. 1–11, 2025.

[21] J.-H. Ewering, Z. Ziaukas, S. Ehlers, and T. Seel, "Reliable State Estimation in a Truck-Semitrailer Combination Using an Artificial Neural Network-Aided Extended Kalman Filter," in *Proc. Eur. Control Conf. (ECC)*, pp. 456–463, Jun. 2024.

[22] T. Gräber, S. Lupberger, M. Unterreiner, and D. Schramm, "A Hybrid Approach to Side-Slip Angle Estimation with Recurrent Neural Networks and Kinematic Vehicle Models," *IEEE Trans. Intell. Veh.*, vol. 4, no. 1, pp. 39–47, Mar. 2019.

[23] C. Nguyen, A.-T. Nguyen, and S. Delprat, "Neural-Network-Based Fuzzy Observer With Data-Driven Uncertainty Identification for Vehicle Dynamics Estimation Under Extreme Driving Conditions: Theory and Experimental Results," *IEEE Trans. Veh. Technol.*, vol. 72, no. 7, pp. 8686–8696, Jul. 2023.

[24] Y. Zhang, Y. Huang, K. Deng, B. Shi, X. Wang, L. Li, and J. Song, "Vehicle Dynamics Estimator Utilizing LSTM-Ensembled Adaptive Kalman Filter," *IEEE Trans. Ind. Electron.*, vol. 72, no. 5, pp. 5429–5439, May. 2025.

[25] Y. Wang, F. Hu, C. Tian, P. Li, H. Huang, G. Yin, and C. Huang, "FTEKFNet: Hybridizing Physical and Data-driven Estimation Algorithms for Vehicle State," *IEEE Trans. Intell. Veh.*, pp. 1–11, 2024.

[26] G. Revach, N. Shlezinger, X. Ni, A. Escoriza, R. van Sloun, and Y. Eldar, "KalmanNet: Neural Network Aided Kalman Filtering for Partially Known Dynamics," *IEEE Trans. Signal Process.*, vol. 70, pp. 1532–1547, 2022.

[27] Q. Li, B. Zhang, H. He, Y. Wang, D. He, and S. Mo, "A Hybrid Physics-Data Driven Approach for Vehicle Dynamics State Estimation," *Mech. Syst. Signal Process.*, vol. 225, no. 112249, pp. 1–19, Feb. 2025.

[28] C. Miao, H. Chu, J. Cao, Z. Sun, and R. Yi, "Steering Angle Adaptive Estimation System Based on GNSS and MEMS Gyro," *Comput. Electron. Agric.*, vol. 153, pp. 196–201, Oct. 2018.

[29] J. Si, Y. Niu, J. Lu, and H. Zhang, "High-Precision Estimation of Steering Angle of Agricultural Tractors Using GPS and Low-Accuracy MEMS," *IEEE Trans. Veh. Technol.*, vol. 68, no. 12, pp. 11 738–11 745, Dec. 2019.

[30] L. Zhang, Z. Wang, X. Ding, S. Li, and Z. Wang, "Fault-Tolerant Control for Intelligent Electrified Vehicles Against Front Wheel Steering Angle Sensor Faults During Trajectory Tracking," *IEEE Access*, vol. 9, pp. 65 174–65 186, 2021.

[31] S. Jeong, T. Kim, and D. Kim, "A Study on Handling Steering Angle Sensor Failure on Redundancy-Based EPS Systems," in *Proc. SAE Int. WCX Congr. Experience*, pp. 1–11, Detroit, USA, Apr. 2024.

[32] J.-Y. Lee, H.-H. Kang, and C.-K. Ahn, "Finite-Memory Front-Wheel Angle Estimation Strategy for Steer-by-Wire System," *IEEE Trans. Ind. Electron.*, vol. 72, no. 2, pp. 2121–2129, Feb. 2025.

[33] A.-T. Nguyen, T.-M. Guerra, C. Sentouh, and J.-C. Popieul, "Decoupling-Based LPV Observer for Driver Torque Intervention Estimation in Human–Machine Shared Driving Under Uncertain Vehicle Dynamics," *IEEE Trans. Autom. Sci. Eng.*, vol. 22, pp. 17 512–17 522, 2025.

[34] H. Ben Moussa and M. Bakhti, "Nonlinear tyre model-based sliding mode observer for vehicle state estimation," *Int. J. Dyn. Control*, vol. 12, no. 8, pp. 2944–2957, Aug. 2024.

[35] H. Alai, A. Zemouche, and R. Rajamani, "Vehicle Trajectory Estimation Using a High-Gain Multi-Output Nonlinear Observer," *IEEE Trans. Intell. Transp. Syst.*, vol. 25, no. 6, pp. 5733–5742, Jun. 2024.

[36] H. Tuan, P. Apkarian, T. Narikiyo, and Y. Yamamoto, "Parameterized Linear Matrix Inequality Techniques in Fuzzy Control System Design," *IEEE Trans. Fuzzy Syst.*, vol. 9, no. 2, pp. 324–332, Apr. 2001.

[37] A. Laub, *Matrix Analysis for Scientists and Engineers*. SIAM, 2004.

[38] T. Karras, M. Aittala, S. Laine, and T. Aila, "Elucidating the Design Space of Diffusion-Based Generative Models," in *Proc. Adv. Neural Inf. Process. Syst. (NeurIPS)*, pp. 565–577, Red Hook, NY, USA, Nov. 2022.

[39] Sustainable and Innovative Mobility and Transport Technopole Valenciennes. The Gyrovia Trail. [Online]. Available: https://www.transalley.com/en/spaces-offices/the-gyrovia-trail

[40] J. Lofberg, "YALMIP : A Toolbox for Modeling and Optimization in MATLAB," in *Proc. IEEE Int. Symp. Comput. Aided Control Syst. Des*, pp. 284–289, Taipei, Taiwan, Sep. 2004.

[41] W. Y. Choi, D. J. Kim, C. M. Kang, S.-H. Lee, and C. C. Chung, "Autonomous Vehicle Lateral Maneuvering by Approximate Explicit Predictive Control," in *Proc. Am. Control Conf. (ACC)*, pp. 4739–4744, Jun. 2018.

[42] A. Fabisch, "gmr: Gaussian Mixture Regression," *J. Open Source Software*, vol. 6, no. 62, pp. 1–4, 2021.

Cheng Tian (Graduate Student Member, IEEE) received his M.Eng. degree in Vehicle Engineering from Tongji University, Shanghai, China, in 2022. He is currently working toward his Ph.D. degree with the Department of Aeronautical and Aviation Engineering, the Hong Kong Polytechnic University, Hong Kong SAR, China. His research interests include vehicle dynamics estimation, safe planning and control for autonomous vehicles.

Anh-Tu Nguyen (Senior Member, IEEE) received the Ph.D. degree in automatic control from the University of Valenciennes, France, in 2013. He is an Associate Professor with INSA Hauts-de-France, Université Polytechnique Hauts-de-France, France. Dr. Nguyen is an Associate Editor for several top-level international journals, including IEEE/ASME TMECH, IEEE T-ITS, IFAC CEP, ISA Transactions. His research interests include robust control and estimation with mechatronics applications.

Edward Chung received his Bachelor's degree and PhD from Monash University. He is a Professor of Intelligent Transport Systems at the Hong Kong Polytechnic University, has extensive experience as an academic and researcher, both domestically and internationally. His research interests include CAV, AI, traffic management and transport modelling.

Hailong Huang (Senior Member, IEEE) received his Ph.D degree in Systems and Control from the University of New South Wales, Sydney, Australia, in 2018. He is now an Assistant Professor at the Department of Aeronautical and Aviation Engineering, the Hong Kong Polytechnic University, Hong Kong. His current research interests include guidance, navigation, and control of UAVs and mobile robots.

He is an Associate Editor of IEEE Transactions on Vehicular Technology, IEEE Transactions on Automation Science and Engineering, Unmanned Systems, Journal of Field Robotics and Intelligent Service Robotics.